# *In Situ* XAFS Analysis of the Reduction and Oxidation Properties of Cu-ZSM-5

M. K. Neylon, C. L. Marshall, A. J. Kropf
Argonne National Laboratory, Argonne, IL, U.S.A.

## Introduction

Within the last 20 years, the use of x-ray absorption spectroscopy has become more popular with catalysis researchers because of its ability to probe in great detail the local structure of catalytically active sites. However, most researchers have run these studies in *ex situ* conditions, in which the state of the catalyst is determined after processing off line. While some studies have also looked at *in situ* XAFS analysis of catalysts, they have typically been limited by both the energy resolution of the beamline and the time required to collect enough significant information. However, we have been able to improve both the resolution and collection speed in order to make *in situ* analysis of catalysis much more feasible while retaining highly detailed results.

In this article, we discuss one example of *in situ* XAFS analysis, the reduction and oxidation properties of Cu-exchanged ZSM-5. This material has been found to be active in the selective catalytic reduction (SRC) of nitric oxides by hydrocarbons [1]; thus, it has received a great deal of attention in the last several years. While a number of other methods, both *ex situ* and *in situ*, have been used to try to probe the nature of copper under various conditions on zeolite [2-4], none of them are as detailed as XAFS. Furthermore, while there have been previous studies of Cu-ZSM-5 during *in situ* XAFS analysis, they lack the resolution that we are able to obtain [5].

## Methods and Materials

Cu-ZSM-5 was prepared by traditional ion exchange methods, by using multiple exchanges of dilute $Cu(NO_3)_2$ (Aldrich) solutions on $NH_4$-ZSM-5 (Zeolyst, $SiO_2/Al_2O_3 = 55$) at room temperature. After each exchange, the samples were calcined in air at 500°C.

*In situ* XAFS analysis was performed in the 10-ID beamline of the Materials Research Collaborative Access Team (MR-CAT). Approximately 40 mg of sample was pressed into a self-supporting wafer (1.5-cm diameter.) and loaded in a 2.56-cm o.d. quartz reactor. A thermocouple was then inserted near the sample in order to track the temperature of the sample. The reactor was sealed with vacuum fittings, and the sample was pretreated for 1 h as listed in Table 1 (gases supplied by AGA Gas). The reactor was then transferred to the hutch and placed in the beam path inside a furnace. Gas lines were connected to the reactor and purged with He.

*Table 1. Gases used during various temperature programmed conditions.*

| Method | Pretreatment | Reaction |
|---|---|---|
| $H_2$ reduction | 5% $O_2$/He | 4% $H_2$/He<br>(or Ar) |
| CO reduction | 5% $O_2$/He | 0.1% CO/He |
| $O_2$ oxidation | 4% $H_2$/He | 5% $O_2$/He |

A cryogenically cooled double-crystal Si(111) monochromator was used to select the beam energy, and a Rh-coated mirror was used to reduce harmonics. The undulator gap was tapered to broaden the bandwidth over the range of the EXAFS scan. The experiment was run in transmission mode; the incident intensity detector was filled with a 50% mixture of nitrogen and helium, and the transmission detector was filled with 80% nitrogen and 20% argon. A copper foil reference spectrum was taken with every scan for energy calibration.

After aligning the beam through the sample, the gas lines were switched to either the reductant or oxidant and allowed to purge through the reactor for 10 min. The furnace was then closed and programmed to heat the sample from room temperature to 600°C at ~3°C/min; simultaneously, XAFS collection was started, cycling between XANES and EXAFS regions along the Cu K edge until the end of the run. After the run and sufficient cooling, the gas lines from the sample were disconnected and the sample was removed, and the furnace was allowed to cool to room temperature before the next experiment.

Several methods of data analysis were performed. First, in all cases, energy calibration was performed by minimizing the error between the normalized Cu foil reference spectra for each XANES and EXAFS data point for a typical accuracy of ±0.05 eV. For EXAFS analysis, standard tools were then used: AUTOBK was used to remove the background signal, and FEFFIT was used to fit the EXAFS signal to predicted paths for various Cu species. The XANES spectra were analyzed by normalizing the edge steps to 1, then using cubic splines to place each spectrum on the same energy grid. Factor analysis [6] was then used to determine the number of significant factors, and iterative key set factor analysis and further refinement were used to determine the key factors.

Selected temperature programs were repeated by using *ex-situ*-temperature-programmed analysis on an Altamira AMI-1 flow-through system. Samples were pretreated and reacted under conditions similar to those listed in Table 1. A thermal conductivity detector was used to analyze the effluent gas.

## Results

The changes in the Cu K XANES spectra during $H_2$, CO, and $O_2$ treatments are shown in Fig. 1. For $H_2$ and CO treatments, the initial material is mostly $Cu^{2+}$, as indicated by the shoulder near 8987 eV. During $H_2$ reduction, $Cu^{1+}$ is formed from $Cu^{2+}$ around 200°C, leading to the strong pre-edge feature at 8983 eV, and then converted to $Cu^0$ by 400°C. During CO reduction, only the conversion of $Cu^{2+}$ to $Cu^{1+}$ is observed near 450°C. For the $O_2$ treatment, the initial material is nearly all $Cu^0$ and is converted to $Cu^{2+}$ with no apparent $Cu^{1+}$ intermediate at temperatures near 250°C.

Fitting of the EXAFS data for the $H_2$ reduction has been done on similar data previously collected at the APS by using similar high-resolution/high-throughput data. Fitting the data over the range of R from 1.0 to 2.7Å, as shown in Fig. 2, allowed for quantitative analysis of three major paths: a short path (R = 1.9Å) typical of Cu-O bonds in CuO, a longer Cu-O path (R = 2.7Å) representing Cu-O-Cu bridging species that may exist in Cu-ZSM-5, and Cu-Cu bonds (R = 2.5Å) found in Cu metal clusters. As reduction proceeds starting near 160°C, the coordination of the Cu-O bonds decreases; the second Cu-O shell disappears as Cu-Cu bonds are formed near 400°C; and finally, the bulk of the material is converted to small Cu clusters by 600°C with an approximate particle size of 5-6 Å, in agreement with the typical pore size of ZSM-5.

By using factor analysis on the $H_2$ temperature-programmed reduction (TPR) data set, we have determined that at least four factors are necessary to describe all spectra with a 95% confidence level. Through iterative key factor analysis and refinement, two of the states were found to correspond to $Cu^{2+}$ and $Cu^0$ species. Two addition states appear to be different forms of $Cu^{1+}$ (referred to as $Cu_{4A}$ and $Cu_{4B}$); they differ in their local coordination. The amount of each state is shown in Fig. 3.

In order to compare the *in situ* XAFS analysis of $H_2$ reduction, we have also run this material in the *ex situ* Altamira system to observe the consumption of hydrogen during reaction. Three major peaks can be deconvoluted from the resulting trace, corresponding to events at 180°, 210°, and 400°C. When this is compared with the XANES, factor analysis, and FEFFIT results, as shown in Fig. 3, we see that these events correlate well with the reduction of $Cu^{2+}$ to various forms of $Cu^{1+}$ and then the final reduction of $Cu^{1+}$ to $Cu^0$. The distinction between the two low-temperature peaks appears to be the type of $Cu^{2+}$ that is reduced, a strong indication that there are at

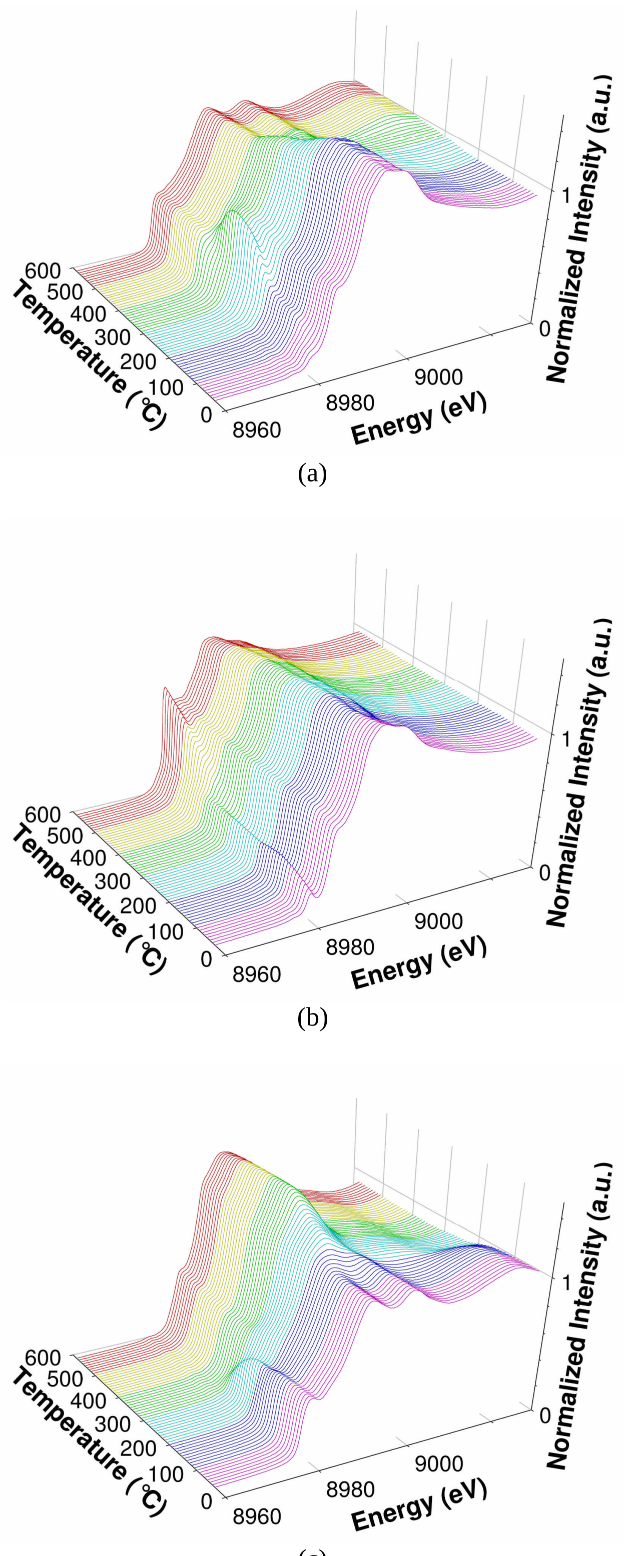

(a)

(b)

(c)

*FIG. 1. Cu K-edge XANES spectra collected during temperature-programmed reactions on Cu-ZSM-5. (a) shows $H_2$ reduction, (b) shows CO reduction, and (c) shows $O_2$ oxidation.*

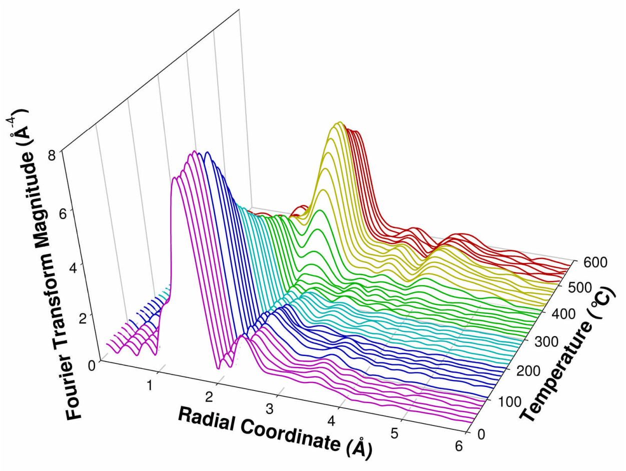

*FIG. 2. Fourier transform of EXAFS function at Cu K edge for Cu-ZSM-5 during $H_2$ TPR.*

least two types of sites on ZSM-5 on which Cu can be stabilized: a five-membered ring and a six-membered ring. Small CuO clusters that can be formed during synthesis may also be reduced, but these should be reduced directly to Cu metal, and the lack of any significant Cu-Cu formation suggests that any CuO present is at undetectable levels.

## Discussion

By using a combination of *ex situ* characterization and *in situ* XAFS analysis, we investigated the local structure of Cu in Cu-ZSM-5 during three reactive systems and correlated changes in the data to the transformations between these states. Copper is initially present on these materials as $Cu^{2+}$ in at least two different sites. These can be easily reduced to $Cu^{1+}$ at moderate temperatures by CO. During reduction in $H_2$, both forms of $Cu^{2+}$ are reduced to $Cu^{1+}$, then subsequently reduced to small $Cu^0$ particles on the zeolite. Upon oxidation of reduced Cu-ZSM-5, there is some $Cu^{1+}$ formation, but it is not of the same nature as the intermediate $Cu^{1+}$ seen during $H_2$ reduction; this intermediate is quickly converted to $Cu^{2+}$. Because the transformation between oxidized and reduced states does not proceed along the same pathway, it is expected that the reduction of Cu-ZSM-5 would have some irreversible component to it. This expectation is supported by the fact that originally isolated Cu appears to migrate to form $Cu^0$ clusters on ZSM-5. This irreversibility and how to avoid it may be a key concept in developing improved SCR catalysts from Cu-ZSM-5.

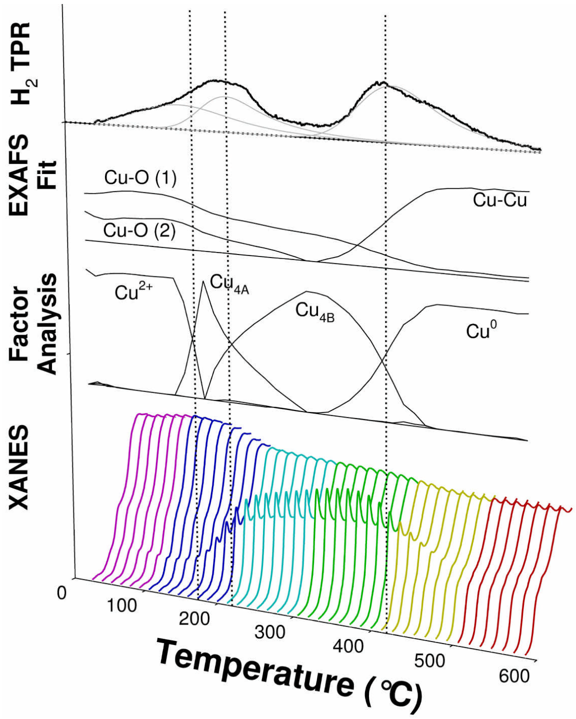

*FIG. 3. Combined results of XANES spectra, factor analysis, EXAFS fitting, and $H_2$ TPR on Cu-ZSM-5.*

## Acknowledgments

Use of the APS was supported by the U.S. Department of Energy (DOE), Office of Science, Office of Basic Energy Sciences, under Contract No. W-31-109-ENG-38. Work performed at MR-CAT is supported in part by funding from DOE under Grant No. DEFG0200ER45811. We wish to thank the staff at MR-CAT for their technical help during testing and setup.

## References

[1] M. Shelef, Chem. Rev. **95**, 209-225 (1995).

[2] T. Beutel, J. Sárkány, G. D. Lei, J. Y. Yan, and W. M. H. Sachtler, J. Phys. Chem. **100**, 845-851 (1996).

[3] R. Kumashiro, Y. Kuroda, and M. Nagao, J. Phys. Chem. B **103**, 89-96 (1999).

[4] G. Turnes Palomino, P. Fisicaro, S. Bordiga, A. Zecchina, E. Giamello, and C. Lamberti, J. Phys. Chem. B **2000**, 4064-4073 (2000).

[5] A. Yamaguchi, Y. Inada, T. Shido, K. Asakura, M. Nomura, and Y. Iwasawa, J. Synchrotron Rad. **8**, 654-656 (2001).

[6] E. R. Malinowski, *Factor Analysis in Chemistry*, 2nd ed. (John Wiley and Sons, New York, NY, 1991).